Check for updates

APPLIED SCIENCES AND ENGINEERING

Nanoscale acoustic oscillator for mechanoimmunology: NAOMI

Ye He[1]†, Ke Jin[1]†, Bo Pan[2,3], Ke Li[1], John D. H. Mai[4], Xianchen Xu[1], Ying Chen[1], Zhiteng Ma[1], Kaichun Yang[1], Shujie Yang[1], Kilian Shambaugh[5], Mingyuan Liu[6], Jianping Xia[1], Yuqi Wu[1], Luke P. Lee[7,8,9,10,11]*, Tony Jun Huang[1]*

Copyright © 2025 The Authors, some rights reserved; exclusive licensee American Association for the Advancement of Science. No claim to original U.S. Government Works. Distributed under a Creative Commons Attribution NonCommercial License 4.0 (CC BY-NC).

Mechanoimmunology explores how mechanical forces orchestrate immune responses, offering insights into immune cell functions and the mechanisms underlying mechanotransduction. A critical challenge in this field is the absence of reliable platforms that apply precise, consistent mechanical stimuli to individual cells while enabling reproducible immune activation. Here, we present a nanoscale acoustic oscillator for mechanoimmunology applications: NAOMI. NAOMI features micropatterned pillars that support uniform cell monolayer formation with an integrated acoustic transducer that delivers highly controlled 3D nanoscale oscillations (±1-nanometer deviation) for up to 72 hours. Unlike conventional passive platforms relying on static stiffness or surface topography, NAOMI enables dynamic, programmable stimulation with high precision and reproducibility. Validation studies demonstrate that NAOMI notably enhances mechanical stress intensity and cell displacement, driving robust M1 polarization in macrophages. NAOMI provides a practical and versatile platform for studying mechanoimmunology, offering high precision, stability, and tunability. Its capabilities also position it well to support future research and drive innovative discoveries in the field.

INTRODUCTION

Human physiological activities and disease progression are often marked by dynamic changes in multiscale biological and biophysical properties. For instance, tissue stiffening during tumor invasion and reduced cell elasticity during cellular aging are well-documented phenomena (*1*–*3*). Immune cells, as central components of the body's defense and homeostatic regulation systems, have an inherent ability to sense these biophysical cues, enabling them to perform immune surveillance and regulate physiological functions (*4*–*6*). This mechanosensitivity is crucial for maintaining their normal function (*7*). For example, mechanical forces have been shown to activate lymphocytes by stimulating T cell antigen receptors or B cell antigen receptors (*8*). Similarly, mechanical stimulation can influence the activation of innate immune cells such as macrophages, dendritic cells, and neutrophils (*9*). These insights highlight the growing importance of the emerging field of mechanoimmunology, which investigates how mechanical stimuli influence immune cell behavior and function.

Despite its potential, our understanding of how different forms of mechanical stimuli specifically affect diverse immune cells and the underlying molecular mechanisms remains incomplete. Most current immunotherapies primarily focus on biochemical cues to enhance immune cell efficacy. Advancing our knowledge in cellular mechanobiology through the framework of mechanoimmunology could pave the way for innovative engineering strategies to modulate immune cell functions more efficiently, effectively, and sustainably.

There are now two main approaches to studying mechanoimmunology. The first uses the extensive interactions between immune cells and the extracellular matrix (ECM) by designing materials with tailored physical features—such as stiffness, Young's modulus, surface topography, spatial confinement, wettability, and roughness—to examine their effects on immune cells (*10*–*16*). The second approach uses engineering techniques to apply dynamic mechanical loading or physical force fields, such as cyclic strain and shear stress, which have been shown to effectively induce macrophage polarization (*17*–*19*). Physical fields, including magnetic, electric, and fluidic flow fields, have also been used to dynamically stimulate immune cells, influencing their a dhesion, activation, and migration (*20*–*24*). While these methods have provided valuable insights, they have several limitations. Material-based methods often require complex fabrication and surface modification processes to mimic ECM mechanics (*25*, *26*), and their physical properties are difficult to tune flexibly across a broad range. Strategies for introducing dynamic behavior, such as material degradation or responsiveness to external stimuli, further complicate precision control. Moreover, the mechanisms by which material physical cues translate into intracellular signaling in immune cells remain poorly understood (*27*). Force field–based systems also face challenges: Magnetic and electric stimulations often depend on exogenous tags or electrochemical interfaces that may introduce confounding factors. Additionally, fluidic flow, while capable of generating shear forces, lacks the spatial confinement and resolution necessary for subcellular mechanotransduction studies (*28*, *29*).

Recently, acoustics and acoustics-induced vibrations have demonstrated strong potential as in vitro stimulation tools to regulate cellular functions and investigate mechanobiology-related pathways (*30*–*35*). These systems allow easy modulation of input parameters—such as resonance frequency, amplitude, and vibration mode—facilitating

[1]The Thomas Lord Department of Mechanical Engineering and Materials, Duke University, Durham, NC 27708, USA. [2]Department of Pharmacology and Cancer Biology, Duke University School of Medicine, Durham, NC 27710, USA. [3]Duke Cancer Institute, Duke University School of Medicine, Durham, NC 27710, USA. [4]Alfred E. Mann Department of Biomedical Engineering, University of Southern California, Los Angeles, CA 90089, USA. [5]Polytec Inc., Irvine, CA 92618, USA. [6]Department of Electrical and Computer Engineering, Duke University, Durham, NC 27708, USA. [7]Harvard Medical School, Harvard University; Renal Division and Division of Engineering in Medicine, Department of Medicine, Brigham and Women's Hospital, Boston, MA 02115, USA. [8]Department of Bioengineering, University of California, Berkeley, Berkeley, CA 94720, USA. [9]Department of Electrical Engineering and Computer Science, University of California, Berkeley, Berkeley, CA 94720, USA. [10]Department of Biophysics, Institute of Quantum Biophysics, Sungkyunkwan University, Suwon 16419, Korea. [11]Department of Chemistry and Nano Science, Ewha Womans University, Seoul 03760, Korea.
*Corresponding author. Email: lplee@bwh.harvard.edu (L.P.L.); tony.huang@duke.edu (T.J.H.)
†These authors contributed equally to this work.

Downloaded from https://www.science.org at EWHA Womans University on December 02, 2025

the study of how dynamically tunable physical cues influence cellular behavior. However, a major limitation of most current acoustic and vibration platforms is their lack of uniformity, spatial precision, and long-term mechanical stability in delivering consistent force at targeted cellular or subcellular locations. For instance, low-frequency, low-intensity pulsed ultrasound (LIPUS), one of the most commonly used acoustic stimulation methods, has been shown to affect various cell types (*36*). Yet, its biological effects remain poorly understood due to the inconsistency of LIPUS-induced acoustic forces across the cell population, the lack of wavelength resolution for subcellular targeting, and potential unintended interference with cellular signaling pathways (*36*–*38*). Considering immune cells are highly mechanosensitive, these limitations notably hinder the potential of current acoustics and vibration platforms for mechanoimmunology research. These issues are particularly critical for mechanoimmunology research, as immune cells are highly mechanosensitive and sensitive to even subtle variations in their mechanical microenvironment. Acoustic force spectroscopy is an emerging platform that enables highly controlled force application at the single-molecule level (*39*). While primarily used to probe molecular interactions, its principles hold promise for subcellular-resolution cell stimulation. However, its current single-cell format limits scalability, throughput, and integration, making it unsuitable in its present form for high-throughput mechanoimmunology applications.

In this study, we introduce nanoscale acoustic oscillator for mechanoimmunology (NAOMI), a platform designed to uniformly modulate immune cell function through precise and stable acoustic stimulation. NAOMI delivers contact-free, label-free, and spatially tunable mechanical signals with high temporal precision, eliminating the need for magnetic labeling or surface functionalization. Mechanical energy is transmitted directly via acoustic pressure fields that naturally interact with cell membranes and the surrounding ECM. This enables localized, oscillatory stimulation within physiologically relevant ranges, allowing for reproducible and biologically meaningful modulation of immune cell behavior at both cellular and subcellular levels. We confirmed that NAOMI transmits nanoscale acoustic waves uniformly to adherent cells, with tunable input parameters and treatment durations. Applying NAOMI to macrophages, we observed strong M1 polarization, accompanied by the up-regulation of integrin family genes, suggesting enhanced cell-substrate interactions after stimulation. Ultimately, polarized M1 macrophages exhibited notably increased phagocytic activity and improved tumor cell–killing efficiency.

RESULTS

Design and operation of the NAOMI platform

To create NAOMI, an in vitro mechanobiological cell stimulation platform that applies mechanical loads to cells uniformly and precisely, we engineered a micropatterned silicon substrate to ensure consistent cell adhesion, defined as uniform cell distribution and reproducibility across experiments (figs. S1 and S2). This was achieved by fabricating microfeatures with uniform size, spacing, and aspect ratio (height-to-diameter ratio, 1.2; fig. S3) and by applying oxygen plasma treatment to generate a homogeneous surface chemistry. Coupling acoustic transducers to this substrate allowed acoustically generated, precise nanoscale oscillations to propagate through the micropatterned structures, thereby mechanically stimulating the cells (Fig. 1A). We selected macrophages as a representative immune cell type to demonstrate NAOMI's capability in modulating immune function. Macrophages were seeded on the substrate overnight to form a monolayer. By tuning the input power and stimulation duration, we effectively induced M1 polarization through integrin signaling (Fig. 1B), an effect associated with increased stress intensity and cell motion at the cell-micropattern interface (Fig. 1C).

The fabrication and characterization of the NAOMI platform

The NAOMI platform is fabricated through a few simple steps, ensuring a cost-effective, scalable, and reusable design. Briefly, a silicon substrate was micropatterned using photolithography. Then, an acoustic transducer was fixed on the bottom of the silicon substrate (Fig. 1, D and E). When a voltage was applied, the oscillations of the piezoelectric actuator were transmitted through the integrated substrate and triggered corresponding nanoscale displacements in the micropatterned surface (Fig. 1F). These nano-oscillations were measured using a laser Doppler vibrometer (MSA-600 Micro System Analyzer, Polytec) and showed high tunability and uniformity. First, as seen in Fig. 2A, the structure of the micropatterned silicon substrate is observed by scanning electron microscopy (SEM). The fabricated micropatterned pillars are highly ordered and uniform. The diameter of a single pattern is 10 μm. The spacing or pitch between patterns is also 10 μm. From a three-dimensional (3D) vibrometry analysis, the average displacement of the micropatterned pillars during oscillation had a high level of uniformity, with only ±1 nm of deviation (Fig. 2B). This extraordinary uniformity is also observed from a broader view (which spans the entire substrate) and at a single pattern level (Fig. 2C). This result shows that this in vitro cell stimulation platform can transmit uniform mechanical stimulations to cells. Next, we report that these acoustics-induced nano-oscillations have a measured and mapped 3D oscillation mode. As shown in Fig. 2D, the magnitude of the z direction (indicated by the blue line) is much higher than the x and y directions (green and orange lines). The simulation results further support this finding, as shown in Fig. 1F, where the oscillation-induced structural displacement occurs primarily out of plane rather than in plane. Therefore, this platform mainly transmits mechanical stimulation in a vertical direction. The magnitude peak occurs at a frequency of 5 kHz. We also studied the relationship between the input voltages and resulting oscillations (Fig. 2E). Five different frequencies are used to drive the structural oscillation (5, 10, 15, 25, and 35 kHz). All of them show a voltage-dependent increase in the oscillation magnitude.

Next, we numerically modeled and simulated these uniform 3D oscillations to evaluate their efficiency in mechanically stimulating cells. First, we simulated the nano-oscillations and experimentally measured the oscillations of the cells, micropatterned pillars, and the silicon substrate, respectively (Fig. 2, F and G). There were clear differences among these three targets. We considered that the oscillations would increase the shear stress intensity at the cell-substrate interface and structure-induced cell oscillations. Before conducting experiments on live cells, we performed numerical simulations. As depicted in Fig. 1 (B and C) and fig. S4, after cells adhered to the micropatterned pillars, the dynamic oscillations originating from the base of the acoustic transducer induced nanoscale oscillations in the micropatterned pillars. The nanoscale oscillation also matched the amplitude and frequency of the silicon micropatterned pillars, as the micropatterned pillars' Young's modulus was 160 GPa. Cells have a Young's modulus of ~49 kPa (*40*). Thus, they exhibited a remarkably lower stiffness compared to the supporting micropatterned

Downloaded from https://www.science.org at EWHA Womans University on December 02, 2025

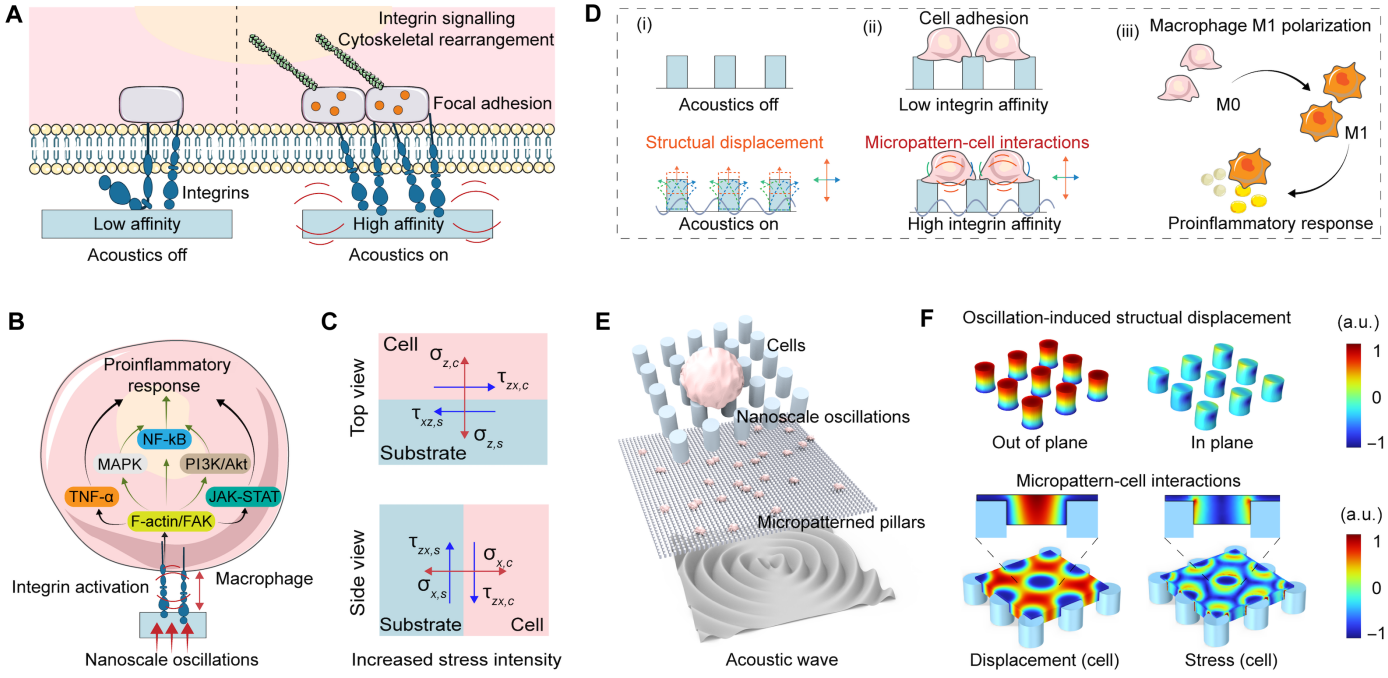


Fig. 1. Schematics of the NAOMI platform and its capabilities in mechanoimmunology. (**A**) NAOMI is capable of delivering steady and uniform nanoscale oscillations to cells and modulating cellular functions through integrin activation. (**B**) The nanoscale oscillations induce macrophage proinflammatory response through integrin and downstream signaling. FAK, focal adhesion kinase; JAK-STAT, Janus kinase–signal transducer and activator of transcription; MAPK, mitogen-activated protein kinase; NF-κB, nuclear factor κB. (**C**) The nanoscale oscillations increase shear stress intensity and cell displacement near the interface of the cell with the micropattern due to the localized displacement induced by the oscillation modes. A detailed explanation of the numerical simulation can be found in fig. S4. (**D**) Schematic of the nanoscale oscillations induced by acoustics can activate integrin and induce M1 polarization of macrophages. (**E**) Acoustic waves applied across the micropatterned substrate induces nanoscale oscillations and delivers mechanical stimulations to the cells. (**F**) Numerical simulation results of the oscillation-induced structural displacement and the increased shear stress intensity and cell displacement near the cell-micropattern interface due to the disparity in oscillation modes. This figure was generated partly using Servier Medical Art, provided by Servier, licensed under a Creative Commons Attribution 4.0 unported license (https://creativecommons.org/licenses/by/4.0/deed.en) (Servier; https://smart.servier.com/).

pillars. When the micropatterned pillars vibrate at the driving frequency of the acoustic transducer, the cells on top experience forced oscillations transmitted mechanically through the micropatterned pillars. Due to their lower stiffness, the cells undergo vibrations with amplitudes that are much larger than the micropatterned pillars. This stiffness mismatch leads to enhanced displacement and stress concentration near the cell-micropillar interface. Both numerical and experimental results (Fig. 1, C and F; fig. S4; and Fig. 2, B and C) confirm that the NAOMI platform generates stable, uniform 3D nanoscale oscillations that are mechanically delivered to the cells, enabling effective mechanical stimulation.

Acoustically induced nano-oscillations enhance M1 polarization of macrophages

We cultured cells from RAW264.7, a murine macrophage cell line, in the NAOMI platform to determine whether the macrophage activities were affected. For cell experiments, ~50,000 RAW264.7 cells were cultured on the micropatterned pillars overnight to allow for thorough cell adhesion. The cell number was determined by forming a cell monolayer on the micropatterned pillars with limited cell overlapping. Next, the acoustics were activated to induce nano-oscillations. This experimental group is denoted as the acoustics-on group. Cells cultured on the micropatterned pillars without nano-oscillations are denoted as the acoustics-off group. Cells cultured on petri dishes are denoted as the petri dish control group. First, we observed the cell viability and morphological changes. As seen in Fig. 3A, according to the live/dead staining result, after 48 hours of treatment, all three groups exhibited good cell viability. Most cells are stained green (alive), and the number of red (dead) stained cells is negligible. Then, we observed the morphological changes by cytoskeleton staining. It was clear that the cells showed a certain level of elongation after being cultured on the micropatterned pillars. The cells maintained their morphology after nano-oscillation treatment. Then, we used a CCK-8 (Cell Counting Kit-8) assay to measure cell viability quantitatively. Figure 3B shows that all groups presented statistically similar viability, consistent with the live/dead staining results. Therefore, cell viability was not significantly affected after being cultured on micropatterned pillars and experiencing 48 hours of nano-oscillation treatment.

Subsequently, to explore whether the cellular functions of the RAW264.7 cells changed, we used several molecular technologies to study macrophage polarization at both the proteomic and genetic levels. First, we used an enzyme-linked immunosorbent assay (ELISA) assay to quantitatively measure the exact secretion concentrations of two proinflammatory markers [tumor necrosis factor–α (TNF-α) and interleukin-1β (IL-1β)] and two anti-inflammatory markers (IL-4 and IL-10). For TNF-α, the acoustics-on group had the statistically highest concentration. The acoustics-off group was also higher than the control petri dish control group. For IL-1β, the concentration of the acoustics-on group was also higher than the

Downloaded from https://www.science.org at EWHA Womans University on December 02, 2025

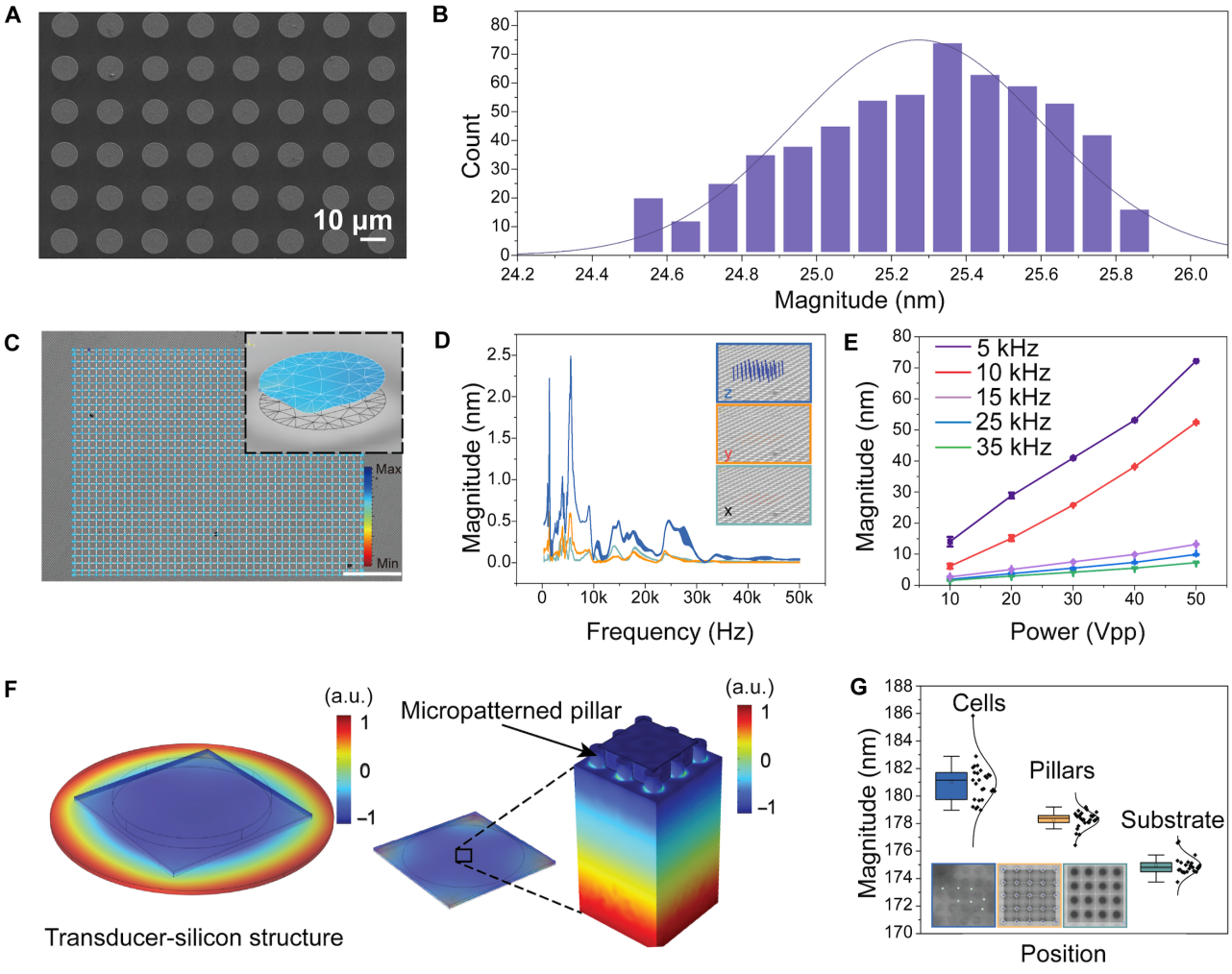


Fig. 2. Device fabrication and characterization of the NAOMI platform. (**A**) A SEM image of the micropatterned pillar arrays (10-μm diameter with 10-μm spacing). (**B**) Vibration analysis histogram of the measured amplitude response of the micropatterns (count, 600), which shows a high level of uniformity during actuation. The average deformation difference between pillars at the nanoscale level is ±1 nm. (**C**) Vibration analysis of the whole micropatterned substrate. The vibration distribution in the whole field and a single pattern (insert image) is uniform. Scale bar, 400 μm. (**D**) 3D vibration characterization of the micropatterns. The amplitudes in the three orthogonal directions (*x*, green line; *y*, orange line; *z*, blue line) are presented for applied acoustic frequencies. (**E**) Response of the vibration amplitudes at five different frequencies with increases in input voltages. (**F**) The numerically simulated result for the displacement distribution of the vibrating NAOMI device, where the silicon structure is on the top. The magnified structure of the silicon structure shows that the bottom actuator drives the oscillation of micropatterned pillars. (**G**) The measured distribution of the vibration amplitudes varies at different positions (i.e., at the cells, top of the micropatterns, and bottom of the substrate).

other two groups. However, the acoustics-off and petri dish control groups had no significant difference. As for IL-4 and IL-10, all three groups had similar secretion levels without significant differences (Fig. 3C). Subsequently, an inflammatory factor array was used to determine the secretion levels of various inflammatory factors qualitatively. As seen in Fig. 3D, there are 27 targets, including 24 proinflammatory factors/chemokines and three anti-inflammatory markers (IL-4, IL-10, and IL-13). According to these results, 21 targets had the highest intensity in the acoustics-on group for proinflammatory factors and chemokines. For the acoustics-off group, only three targets had the highest intensity. For the petri dish control group, all targets had the lowest intensity. As for the anti-inflammatory targets, although the acoustics-on group still had the highest intensity, the differences among the three groups were very small. Then, we used quantitative polymerase chain reaction (qPCR) to detect the gene expression level of eight proinflammatory factors (Fig. 3E). All eight targets were up-regulated in the acoustics-on group, compared to the other two groups. In addition, the gene expression of seven targets in the acoustics-off group was also higher than the petri dish control group. Then, we used flow cytometry to detect the expression of M1 and M2 cell markers. We used CD86 and CD206 as the representative M1 and M2 markers. In Fig. 3F, consistent with the above results, the acoustics-on group has the most CD86-positive cells compared to the other two groups. As for CD206-positive cells, according to the flow cytometry results, the positive number of cells in the acoustics-on group was lower than the other two groups.

We also performed immunofluorescence staining to visualize the CD86 expression levels in all three groups. As shown in Fig. 3G, compared to the petri dish control and acoustics-off group, the acoustics-on group exhibited greater CD86 signals. Last, we provided the flow

Downloaded from https://www.science.org at EWHA Womans University on December 02, 2025

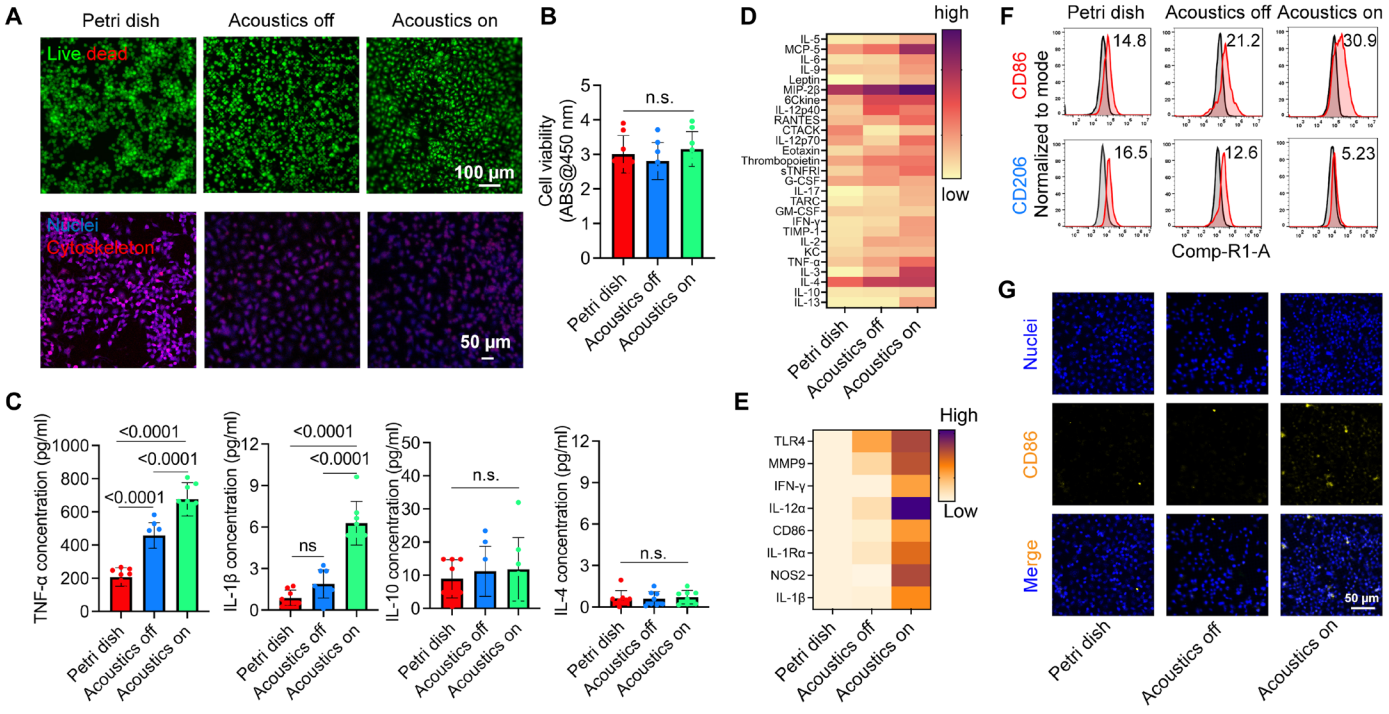


Fig. 3. NAOMI improves M1 polarization of macrophages. (**A**) Optical microscope images of live/dead stained cells and stained cytoskeleton. (**B**) CCK-8 assay measuring cell viability under different experimental conditions (absorbance at 450 nm was measured) ($n = 8$). (**C**) Enzyme-linked immunosorbent assay (ELISA) assay measuring the secretion of tumor necrosis factor–α (TNF-α), interleukin-1β (IL-1β), IL-4, and IL-10 from different groups ($n = 8$). (**D**) Heatmap presenting the secretome profiles of inflammatory factors for different experimental conditions. MIP-2β, macrophage inflammatory protein 2β; G-CSF, granulocyte colony-stimulating factor; GM-CSF, granulocyte-macrophage colony-stimulating factor; IFN-γ, interferon-γ; TIMP-1, tissue inhibitor of matrix metalloproteinase 1. (**E**) Quantitative polymerase chain reaction (qPCR) assay testing the gene expression level of various proinflammatory genes. TLR4, Toll-like receptor 4; MMP9, matrix metalloproteinase 9; NOS2, nitric oxide synthase 2. (**F**) Flow cytometry analysis detecting the percentage of CD86- and CD206-positive cells for the different conditions. (**G**) Immunofluorescence staining images of CD86 signal of different conditions. Statistical analysis was performed using one-way analysis of variance (ANOVA) with Tukey's post hoc test. Cells cultured on flat petri dishes are referred to as the petri dish group, while those on micropatterns with or without nano-oscillations are labeled as the acoustics-on and acoustics-off groups, respectively. Data are presented as means ± SD.

cytometry results at different intervals to explain why 48 hours of acoustic treatment is selected as the best practical treatment time. As shown in fig. S5, cells were treated for 24, 36, and 72 hours, respectively. Then, the expression of CD86 and CD206 was detected by flow cytometry. We found that, after 24 and 36 hours of treatment, the intensity of CD86 in the acoustics-on group remained higher than the other two groups. However, compared to the results of the 48-hour treatment, the difference was much smaller. After 72 hours of treatment, the result was relatively clear, as the CD86 intensity was much higher than the other two groups. However, due to the fast cell proliferation profile of macrophages, a 72-hour cell culture was too long, and the monolayer cell culture was difficult to maintain. Therefore, 48 hours was selected as the most appropriate treatment duration. Overall, these results strongly suggested that the acoustics-induced nano-oscillations can improve the M1 phenotype polarization of macrophages.

NAOMI increased the expression of the integrins family

Because macrophages are effectively polarized to the M1 phenotype, the NAOMI platform has proven capable of regulating cell functions through mechanical stimulations. Accordingly, we explored the underlying molecular mechanisms. We used RNA sequencing (RNA-seq) techniques to study the overall gene expression profile and the changes in specific functional gene groups following the nano-oscillation treatment. Based on the above results, cells in the acoustics-off group had similar M1 polarization levels to the petri dish control group. The M1 polarization of macrophages in the acoustics-on group should, thus, be attributed to the nano-oscillations. Therefore, we collected the mRNA from the acoustics-off and acoustics-on groups and studied the gene expression differences via RNA-seq.

First, we compared the overall gene expression difference. In Fig. 4A, compared to the acoustics-off group, 449 genes were up-regulated, and 147 genes were down-regulated. A total of 13,926 genes were not changed. We have summarized all changed genes in a heatmap (Fig. 4B). Each group has three biological repeats, and we can see that the tendency in each repeat is relatively consistent. Next, Gene Ontology (GO) pathway enrichment analysis was performed to examine cell function and signal pathway changes. In Fig. 4C, compared to the acoustics-off group, the acoustics-on group displays remarkable enrichment in proinflammatory reactions, such as defense responses, positive regulation of innate immune responses, cell chemotaxis, TNF superfamily cytokine production, acute inflammatory response, and macrophage activation. These results verified that macrophages in the acoustics-on group were polarized to the M1 phenotype to have higher proinflammatory responses.

We also found that macrophages in the acoustics-on group presented significant enrichment in cell-substrate interactions compared

Downloaded from https://www.science.org at EWHA Womans University on December 02, 2025

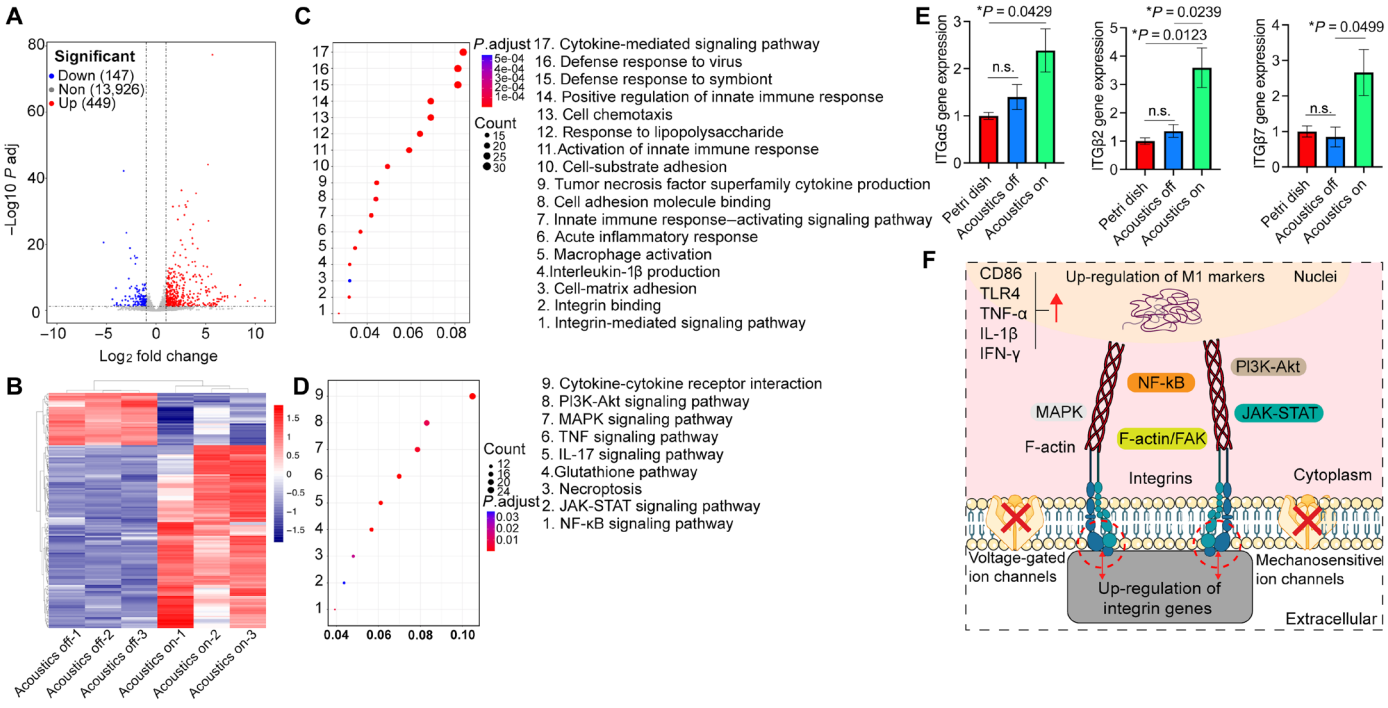


Fig. 4. NAOMI induced proinflammatory response of macrophages through up-regulation of the integrin family. (**A**) Volcano plots showing the differentially expressed genes in each group. (**B**) Heatmaps displaying the differentially transcribed genes of interest in each group. Each group has three biological repeats. (**C** and **D**) Gene Ontology (GO) pathway enrichment analysis and Kyoto Encyclopedia of Genes and Genomes (KEGG) pathway enrichment analysis. (**E**) qPCR assay measuring the gene expression of ITGα5, ITGβ2, and ITGβ7 of each group ($n = 3$). (**F**) Illustration of how NAOMI up-regulated the expression of the integrin family and improved the M1 polarization of macrophages. Statistical analysis was performed using one-way ANOVA with Tukey's post hoc test. Data are presented as means ± SD.

to the acoustics-off group. This includes interactions such as cell-substrate adhesion, cell adhesion molecule binding, integrin binding, and integrin signal pathways. These results demonstrate that after 48 hours of nano-oscillation treatment, macrophages have notably higher interactions with the micropatterned substrate, which may regulate their polarization. Next, Kyoto Encyclopedia of Genes and Genomes (KEGG) pathway enrichment analysis was performed to study which signal pathways were changed considerably. As shown in Fig. 4D, several integrin-mediated signal pathways, such as phosphatidylinositol 3-kinase–Akt, mitogen-activated protein kinase, and nuclear factor κB, have changed remarkably. These results indicate that the up-regulation of the integrin family might be a potential regulator of macrophage M1 polarization. To verify this hypothesis, we examined the gene group of the integrin family. In fig. S6, most genes of the integrin family were up-regulated in the acoustics-on group. We also used qPCR to detect the expression of three integrin markers (ITGα5, ITGβ2, and ITGβ7). In Fig. 4E, the acoustics-on group had statistically the highest expression level of these three markers, and the other two groups had no significant differences. Therefore, it is reasonable to conclude that the integrin family is up-regulated following the nano-oscillation treatment. In addition, we did not observe the enrichment of any well-known mechanical-responsive signal pathways in the RNA-seq results, such as mechanosensitive and voltage-gated ion channels.

Figure S7 summarizes the gene expression profiles, including calcium voltage-gated channels, potassium voltage-gated channels, sodium voltage-gated channels, piezo channels, transient receptor potential cation channels, voltage-dependent anion channels, and chloride voltage-gated channels. We found no significant differences in gene expression between the acoustics-off and acoustics-on groups for any of these pathways. This result is interesting because mechanosensitive ion channels (such as piezo) and voltage-gated channels are well-known to be responsive to various mechanical stimulations, especially acoustics and vibrations. These results showed that only the integrin family is up-regulated, indicating that the nano-oscillations are transmitted to cells through better cell-substrate interaction rather than direct mechanical stimulation pathways (Fig. 4F).

M1-polarized macrophages prepared using NAOMI exhibit enhanced phagocytic capacity and increased tumor cell–killing efficiency

Because M1-polarized macrophages exhibited proinflammatory responses, we next explored the potential therapeutic applications of the nano-oscillation-treated RAW264.7 cells. First, we examined their phagocytosis capacity. Commercially available pHrodo bioparticles and a cell labeling kit were used. The pHrodo bioparticles and labeled cells can only exhibit fluorescence when the environmental pH value is about 4, close to that found within macrophage lysosomes. Therefore, if a fluorescence signal was detected, then the macrophages had already phagocytosed the bioparticles and labeled cells. Here, we labeled suspended Raji tumor cells as the target cells. After collecting RAW264.7 cells from each group, pHrodo bioparticles and labeled Raji cells were cocultured with the RAW264.7 cells for 1, 2, 6, 12, and 24 hours (Fig. 5A). We used both confocal microscopy and flow cytometry to obtain the following results. According to confocal microscopy imaging (Fig. 5, B and C), after 2 hours of

Downloaded from https://www.science.org at EWHA Womans University on December 02, 2025

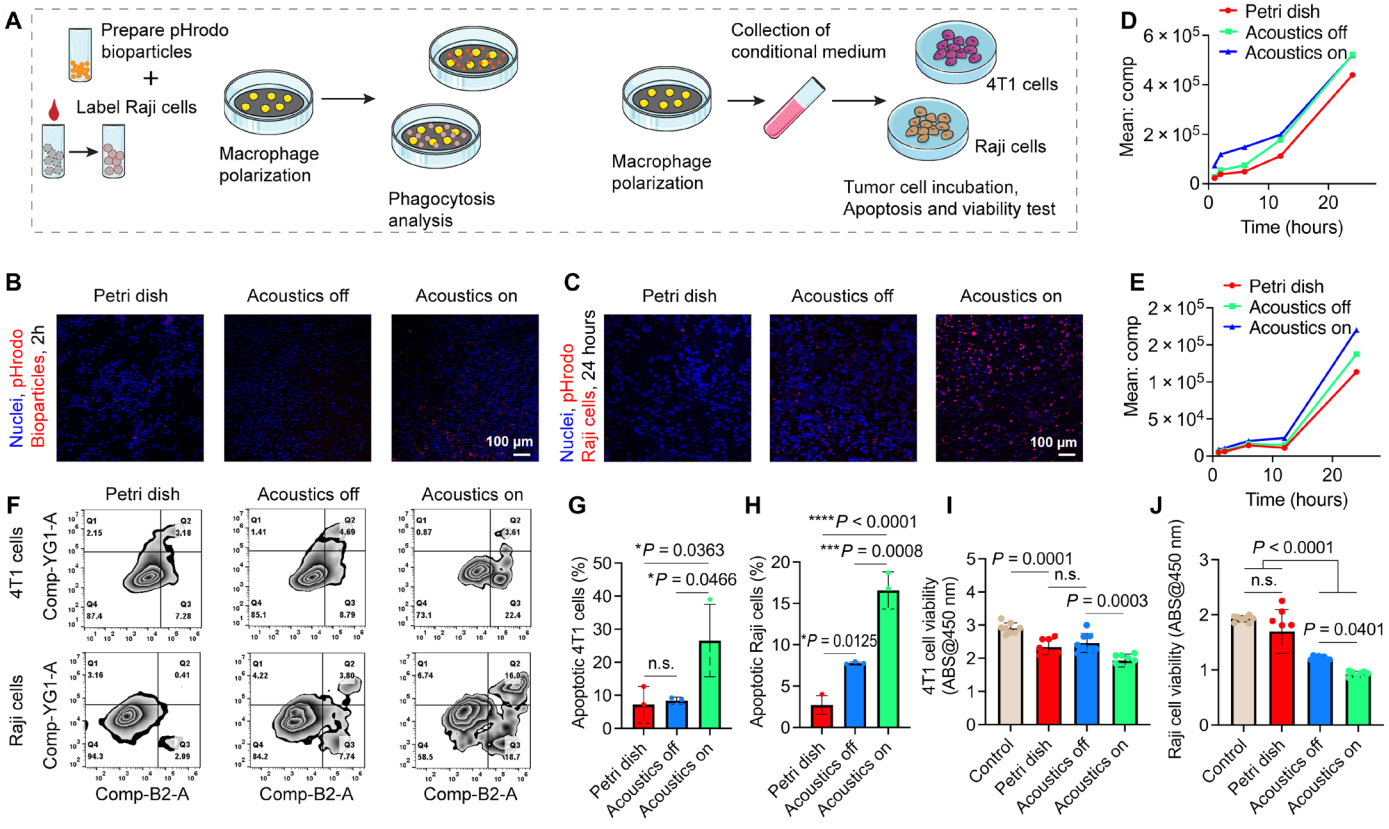


Fig. 5. M1-polarized macrophages have better phagocytosis capacity and tumor cell–killing efficiency. (**A**) Illustrations describing the macrophage phagocytosis analysis and tumor cell–killing efficiency tests. (**B**) Immunofluorescence stained images of macrophage phagocytosis for pHrodo bioparticles after 2 hours of incubation with respect to different experimental conditions. (**C**) Immunofluorescence stained images of macrophage phagocytosis for pHrodo Raji cells after 24 hours of incubation for different groups. (**D** and **E**) Flow cytometry analysis measuring macrophage phagocytosis for pHrodo bioparticles and pHrodo Raji cells after 1, 2, 6, 12, and 24 hours of incubation, with respect to the different experimental conditions. (**F**) Flow cytometry analysis measuring cell apoptosis levels of 4T1 cells and Raji cells after coculturing with the conditional medium from different groups. (**G** and **H**) Statistical summarization of flow cytometry results for cell apoptosis measurement ($n = 3$). (**I** and **J**) CCK-8 assay measuring cell viabilities of 4T1 cells and Raji cells after coculturing with the conditional medium from different groups [absorbance (ABS) at 450 nm was measured] ($n = 8$). Statistical analysis was performed using one-way ANOVA with Tukey's post hoc test. Data are presented as means ± SD. This figure was generated partly using Servier Medical Art, provided by Servier, licensed under a Creative Commons Attribution 4.0 unported license (https://creativecommons.org/licenses/by/4.0/deed.en) (Servier; https://smart.servier.com/).

coculture, it is clear that RAW264.7 cells from the acoustics-on group had the highest phagocytosis capacity for the bioparticles. After 24 hours of coculture, the acoustics-on group also showed excellent phagocytosis capacity for the Raji cells. Then, we used flow cytometry to measure the phagocytosis profile. In Fig. 5 (D and E) and fig. S8, for pHrodo bioparticles, the acoustics-on group exhibits a rapid phagocytosis behavior at the beginning (the first 6 hours). After 24 hours of coculture, all groups showed a similar phagocytosis capacity. As for Raji cells, at the first 6 hours, all groups displayed little differences. However, after 12 hours, the acoustics-on group gradually showed a better phagocytosis capacity.

Subsequently, the tumor cell–killing efficiency was examined. Raji cells were selected as the representative suspended tumor cell type, and 4T1 cells were selected as the representative adherent tumor cell type. The conditional medium from each group was collected to incubate tumor cells for 2 days and observe their viability and apoptosis levels. First, flow cytometry was used to detect the apoptosis level (Fig. 5, F to H). For 4T1 cells, 22.4% were apoptotic in the acoustics-on group. Only 8.79 and 7.28% of cells were apoptotic in the acoustics-off and petri dish control groups. For Raji cells, 18.7% were apoptotic in the acoustics-on group. Only 7.74 and 2.09% of cells were apoptotic in the acoustics-off and petri dish control groups. The flow cytometry test had three biological repeats. According to the statistical analysis, the acoustics-on group had a significantly higher ability to induce apoptosis in both 4T1 and Raji cells. The other two groups exhibited no significant differences. Last, we used a CCK-8 assay to study the cell viability. A control group entailed culturing two tumor cells in their culture medium without adding the conditional medium of macrophages. The results are shown in Fig. 5 (I and J). The viability of both 4T1 and Raji cells is lowest in the acoustics-on group. The acoustics-off group also showed statistically lower viability compared to the control group.

DISCUSSION

The biological functions and fate of immune cells, such as macrophages, are closely related to mechanobiological signals during their entire lifecycles. Immune cells are exposed to mechanical inputs from different tissues, the hydrodynamic forces within circulating systems, and even the pathogenic progressions accompanied by

Downloaded from https://www.science.org at EWHA Womans University on December 02, 2025

physical changes (*27*, *41*). Mechanotransduction is a faster and more effective way to regulate immune cell functions than biochemical cues, triggering timely and appropriate immune reactions. Thus, mechanoimmunology offers a promising and strong future for regulating immune cells. Nevertheless, in contrast to biochemical regulation, the influence of mechanical stimulation on immune cells presents numerous unresolved questions. These include achieving an optimal immunological effect and the molecular mechanisms involved.

To this end, this study presents an acoustically induced nano-oscillation platform, NAOMI, which provides uniform and precise mechanical stimulations to macrophages. The silicon micropatterned pillars serve as focal points for adhesion for macrophages to improve precise mechanotransduction and transmit a uniform mechanical loading to each cell. Traditional mechanical stimulation platforms often struggle to deliver uniform mechanical forces to cells. For instance, in microfluidic devices, mechanical forces rapidly diminish from the center toward the boundaries, while in acoustic devices, pressure waves dissipate as they travel from proximal to distal regions. These limitations remarkably compromise the reliability and consistency of such platforms for studying mechano-immunology. Our NAOMI platform maintains an oscillation magnitude deviation of just ±1 nm across the entire substrate. When a monolayer of macrophages is cultured on NAOMI, each cell experiences uniform mechanical stimulation, greatly enhancing experimental reliability.

While NAOMI exhibits considerable precision and uniformity, several limitations must be recognized. First, the mechanical stimulation is transmitted primarily in a quasi-two-dimensional configuration and does not fully replicate the complex 3D mechanical environment found in native tissues and cells. Second, the operating frequency is constrained by the design of the acoustic transducer and substrate, which may require reoptimization for applications involving suspension cells, organoids, or mechanically distinct tissues, as well as for the selective activation of target organelles or specific molecular pathways. The design of the acoustic transducer is a critical factor that must carefully integrate multiple parameters—including geometry, frequency, power, and vibration mode—to achieve optimal acoustic field performance tailored to specific applications (*42*–*48*). For instance, ring-shaped transducers can generate hollow, annular acoustic fields suitable for localized enhancement. In contrast, rectangular or strip-shaped transducers exhibit good directionality, producing planar acoustic waves that are ideal for uniform stimulation over large areas. Circular transducers have the capability to deliver relatively uniform fields in symmetric configurations. Moreover, the vibration mode (for instance, thickness, shear, or radial) determines the direction of wave propagation and the distribution of energy.

In this study, the chosen transducer structure demonstrated commendable control and uniformity of the acoustic field. Nonetheless, future efforts may aim to further optimize geometric design and vibration modes to improve overall performance. Furthermore, it is worthwhile to investigate how various vibration modes and spatial acoustic distributions affect cellular responses. Additionally, while the platform is theoretically scalable for high-throughput applications, the present utilization of opaque substrates such as silicon limits compatibility with inverted microscopy and live-cell imaging. To address these limitations, we plan to develop transparent substrate variants, including those made from glass, to enhance optical accessibility and facilitate integration with conventional imaging and screening systems. These improvements aim to expand the utility of NAOMI in both fundamental research and translational applications.

Macrophages were chosen as the representative immune cell type for several key reasons. First, as a crucial component of the innate immune system, macrophages play a fundamental role in immune regulation, making the study of their functions and underlying mechanisms highly important. Second, their remarkable plasticity is a defining characteristic, with distinct phenotypes such as M1 and M2, along with subtypes like M2a, M2b, and M2c, each contributing to critical physiological processes (*49*–*51*). However, their high mechanosensitivity has historically introduced experimental variability, as different force types, mechanical dosages, and treatment durations can lead to divergent outcomes. Given these factors, macrophages provide both a practical and clinically relevant model for evaluating our NOAMI platform's stability and reproducibility while offering a reliable method for precisely regulating macrophage functions.

Our results showed that, while cell morphology changed in the acoustics-off group, integrin family gene expression did not exhibit statistically significant up-regulation compared to cells cultured in petri dishes, suggesting that the micropatterned pillars alone were insufficient to induce substantial changes in integrin expression. However, after 48 hours of nano-oscillation treatment, integrin family gene expression was significantly up-regulated. The expression of several commonly reported protein channels, including mechanosensitive ion channels and voltage-gated channels, remained unchanged. This suggests that nano-oscillation treatment primarily enhances macrophage interactions with the micropatterned pillars to regulate cell functions rather than directly stimulating cells through mechanical forces, which aligns with the fact that nano-oscillation is a relatively gentle form of mechanical stimulation. Integrins, extensively reported to mediate cellular responses to mechanical stimuli, have been implicated in similar mechanisms; for instance, a previous study demonstrated that a microbubble system attaching to cells via integrins influenced stem cell differentiation when exposed to ultrasound-induced microbubble vibrations (*52*, *53*). Similarly, other studies have shown that vibration-induced cell differentiation and adhesion are largely attributed to integrin activity, further supporting our findings (*54*–*56*).

Last, we examined the therapeutic potential of macrophages following NAOMI treatment. Our findings indicated that macrophages were polarized to the M1 phenotype, resulting in increased release of proinflammatory factors. Consequently, we investigated their phagocytic capacity and ability to kill tumor cells efficiently. Previous studies reported that macrophages with different phenotypes may present distinct phagocytosis profiles (*57*, *58*). M1 macrophages can be rapidly activated by pathogens. In our study, they demonstrated a swift and robust phagocytic response against bioparticles (bacteria) and sustained superior phagocytic activity against tumor cells, aligning with previous findings. In addition, we observed distinct phagocytic dynamics toward bacterial bioparticles and tumor cells. For bacterial targets, the acoustics-on group exhibited a rapid initial response, but the difference among groups diminished by 24 hours, likely because unactivated (M0) macrophages still retain baseline phagocytic capacity and gradually internalize bacteria over time. In contrast, tumor cell phagocytosis showed a sustained enhancement in the acoustics-on group throughout the entire time course, suggesting a more persistent effect. This difference likely reflects the inherent complexity of tumor cell clearance, which

Downloaded from https://www.science.org at EWHA Womans University on December 02, 2025

generally requires stronger activation cues, prolonged engagement, and enhanced expression of phagocytic receptors. Therefore, while NAOMI primarily accelerates early-stage phagocytosis of readily recognized targets like bacteria, it appears to accelerate and amplify macrophage-mediated clearance of more challenging targets such as tumor cells. Furthermore, M1 macrophages effectively targeted both adherent and suspended tumor cells, inducing apoptosis with high efficiency. These results underscore the potential of the NAOMI platform for generating M1 macrophages as a powerful therapeutic strategy against cancer and infectious diseases.

MATERIALS AND METHODS

Device fabrication

Our device features a reconfigurable sandwich-style assembly composed of three main components: silicon micropatterned pillars, a modified petri dish serving as a bioreactor, and an acoustic transducer. Each element can be independently assembled and reconfigured based on experimental needs (figs. S1 to S3). The silicon micropatterned pillars were created through photolithography and subsequently bulk-etched using deep reactive ion etching. A silicon wafer with 500 μm thickness was first spin coated with a positive photoresist (Shipley S1813, Marlborough, MA). Then, it was patterned, exposed, and developed to form 10-μm circles. After cleaning and drying, a Pegasus deep silicon etcher (SPTS Technologies) was used to etch the structure into the silicon micropatterned pillars. After that, the silicon wafer was diced into silicon plates (175 mm by 175 mm). We developed a platform by replacing the glass bottom of a polystyrene culture dish (Nest Scientific 801002, Jiangsu, China) with fabricated silicon micropatterned pillars. The space between the silicon micropatterned pillars and the culture dish was filled with poly(dimethylsiloxane) and cured at 65°C, ensuring biocompatibility and soft sealing. The micropattern aspect ratio (height to diameter) was maintained at 1.2. Last, an acoustic transducer (PUI Audio AB2746B-LW100-R, Fairborn, OH) was securely attached to the bottom of the silicon plate using an epoxy bond. A portable signal generator i(GH-CJDS66-A, Koolertron) is used to power the NAOMI bioreactor which can be easily placed in cell culture incubator.

Vibration measurement

A microscope-based laser vibrometer was used to assess nanometric displacements. Two Micro System Analyzers (MSA-500-3D and MSA-600, Polytec) were used to measure the 2D and 3D vibrations, respectively. A laser beam mounted on a movable stage can be focused on targeted spots to track their position and velocity accurately. In-plane and out-of-plane deformation and vibration modes were recorded with nanometer amplitude resolutions. The frequencies were set to 5 kHz. During the vibration experiments, we applied a peak-to-peak voltage of 18 Vpp. The detection area was ~3 mm^2, which corresponds to about $^1/_{20}$ of the total usable stimulation region. This area represents the maximum field of view achievable with the 5× objective of the vibrometer and was selected to ensure consistency across measurements and to support the statistical relevance of the analyzed region. The data were processed and analyzed with PSV (10.2) software.

Cell culture

Cryopreserved RAW264.7 murine macrophage cell line, lymphoblast-like Raji cell line, and 4T1 cell line were obtained from American Type Culture Collection (ATCC; TIB-71, CCL-86, CRL-2539). Cells were cultured in Dulbecco's modified Eagle's medium culture medium (ATCC 30-2002, for RAW264.7 cells) and RPMI-1640 medium (ATCC 30-2001, for Raji cells and 4T1 cells), with 10% of fetal bovine serum (v/v) under a 5% CO_2 atmosphere at 37°C. The medium was replaced on the first day and every 2 days thereafter. Cells in the third passage were used in this study.

Sample preparation

Before cell experiments, the devices were ultrasonically cleaned with ethanol and distilled water and sterilized by UV light overnight. Next, a 250-μl droplet of suspended RAW264.7 cells (~5×10^4 cells) was added to each device. Then, the cell samples were cultured overnight in a cell incubator to allow cell attachment. After that, the devices were connected to function generators. After turning the acoustics on, each sample was treated for 48 hours. The acoustic parameters were set to a peak-to-peak voltage of 18 V and a frequency of 5 kHz. The cell samples were cultured for 48 hours without acoustics for the petri dish control and acoustics-off groups.

Cell morphology observation

To observe cell morphology, after 48 hours of treatment, RAW264.7 cell samples were stained by a Phalloidin-iFluor 555 Reagent (Abcam, ab176756) and Hoechst 33342 (Invitrogen, H3570). Then, the samples were imaged using an upright confocal microscope (Zeiss 780).

Cell viability evaluation

First, to visually observe cell viability, after 48 hours of treatment, RAW264.7 cell samples were labeled with the LIVE/DEAD Viability/Cytotoxicity Kit (Invitrogen, L3224) and imaged using the upright confocal microscope (Zeiss 780). Second, a CCK-8 assay was performed to study cell viability quantitatively. In brief, a 10% (v/v) CCK-8 working solution (GlpBio, GK10001) was mixed into the cell culture medium. After a 2-hour incubation period, the mixture was measured by a spectrophotometric microplate reader (BioTek Instruments Inc.) at 450 nm.

Phenotype switch studies of RAW264.7 cells

For flow cytometry analysis, RAW264.7 cells were incubated with a Pacific Blue anti-CD86 antibody (BioLegend, 105021) and a fluorescein isothiocyanate anti-CD206 antibody (BioLegend, 141703) for 30 min, respectively. After incubation, the cells were analyzed by flow cytometry (BD Biosciences, USA). For protein array assay, the supernatant of each sample was collected and incubated with an inflammatory cytokine array (Abcam, ab133994) according to the manufacturer's instructions. For the cytoimmunofluorescence staining, the cell samples were fixed with 4% paraformaldehyde, permeabilized by 0.2% Triton X-100, and blocked with a 1% bovine serum albumin solution. After that, the CD86 antibody (Abcam, ab119857) was used to stain cells. Cell nuclei were stained using Hoechst 33342. Then, the samples were imaged by the upright confocal microscope (Zeiss 780). For qPCR testing, the qPCR array kits were provided by ScienCell Research Laboratories (Carlsbad, CA, USA). cDNA first-strand synthesis and PCR amplification were carried out following the manufacturer's instructions. The CFX Duet Real-Time PCR System (Bio-Rad) detected and analyzed the results. For ELISA tests, the secretion of TNF-α, IL-1β, IL-4, and IL-10 was measured by Mouse TNF alpha ELISA Kit (Abcam, ab208348), Mouse IL-1 beta ELISA Kit (Abcam, ab197742), Mouse IL-4 ELISA Kit (Abcam,

Downloaded from https://www.science.org at EWHA Womans University on December 02, 2025

ab100710), and Mouse IL-10 ELISA Kit (Abcam, ab100697), respectively.

RNA-seq analysis

After 48 hours of treatment, RAW264.7 cell samples were collected and frozen rapidly. Then, the RNA extraction and high-throughput sequencing were performed by GENEWIZ from Azenta US Inc. (USA). For the data analysis, the fastQ files of mouse cell RNA-seq data were trimmed and filtered using Trim Galore (v.0.6.8). Then, they were aligned to the GRCm38/mm10 mouse genome using STAR (v.2.7.11) with the following parameters: outSAMtype BAM Unsorted- quantMode TranscriptomeSAM. The transcript abundance for each sample was estimated using salmon (v.1.4.0) to quantify the transcriptome defined by Gencode vM25. Gene level counts were summed across isoforms, and genes with low counts (maximum expression < 10) were filtered out from downstream analyses. We tested genes for differential expression in DESeq2 (v.1.38.2) in R, and GO/KEGG analysis was performed using clusterProfiler (v.3.10.1) package in R. The heatmap (v.1.0.12) package produced the heatmaps of gene expressions. Next-generation sequencing data have been deposited into the NCBI's Gene Expression Omnibus database under accession number GSE303278.

qPCR test for the integrin family

ScienCell Research Laboratories (Carlsbad, CA, USA) provided the qPCR kits. cDNA first-strand synthesis and PCR reaction were performed according to the manufacturer's instructions. The CFX Duet Real-Time PCR System (Bio-Rad) detected and analyzed the results.

Macrophage phagocytosis analysis

pHrodo Cell Labeling Kit and pHrodo Bioparticles for Incucyte Phagocytosis Assays were purchased from Sartorius Co. (USA). Raji cells were labeled according to the manufacturer's instructions for cell labeling. To perform the phagocytosis analysis, RAW264.7 cells of each group were collected and incubated with the pHrodo Raji cells and bioparticles for 1, 2, 6, 12, and 24 hours, respectively. Then, the RAW264.7 cells were cleaned and centrifuged according to the manufacturer's instructions and detected by the upright confocal microscope (Zeiss 780) and flow cytometry (BD Biosciences, USA).

Tumor cell–killing efficiency assays

We selected 4T1 and Raji cells as the representative adherent and suspended cell types. To test the killing efficiency of macrophages, first, the culture medium of RAW264.7 cells from each group was collected and centrifuged to remove cells. After that, the medium of each group was mixed with the medium of 4T1 cells and Raji cells (1:1), respectively, to prepare the conditional medium. Then, 4T1 and Raji cells were cultured for 2 days using the conditional medium. Next, the cell apoptosis level was detected by flow cytometry (BD Biosciences, USA). Cell viability was assessed by CCK-8 assay, as described before.

Statistical analysis

All statistical analyses were performed with one-way analysis of variance (ANOVA) and Tukey's post hoc test using GraphPad Prism 9.0. All images were processed by ImageJ (National Institutes of Health, USA). The data are presented as means ± SD of multiple biological replicates, as indicated in the figure legends. For qPCR results, the data were processed by CFX Maestro Software for CFX Real-Time PCR Instruments and presented as normalized expression ± expression SEM. n.s., not significant.

AI use

Portions of this manuscript were refined with assistance from OpenAI's ChatGPT (GPT-4). Prompts used included "Improve text conciseness," "Improve text clarity," and "Refine the abstract's flow." All AI-assisted edits were critically reviewed, revised, and approved by the authors.

Supplementary Materials

This PDF file includes:

Figs. S1 to S8

Supplementary Text for fig. S4

REFERENCES AND NOTES

1. H. Mohammadi, E. Sahai, Mechanisms and impact of altered tumour mechanics. *Nat. Cell Biol.* **20**, 766–774 (2018).
2. J. M. Phillip, I. Aifuwa, J. Walston, D. Wirtz, The mechanobiology of aging. *Annu. Rev. Biomed. Eng.* **17**, 113–141 (2015).
3. E. H. Barriga, K. Franze, G. Charras, R. Mayor, Tissue stiffening coordinates morphogenesis by triggering collective cell migration in vivo. *Nature* **554**, 523–527 (2018).
4. V. Mittelheisser, V. Gensbittel, L. Bonati, W. Li, L. Tang, J. G. Goetz, Evidence and therapeutic implications of biomechanically regulated immunosurveillance in cancer and other diseases. *Nat. Nanotechnol.* **19**, 281–297 (2024).
5. H. Bai, L. Si, A. Jiang, C. Belgur, Y. Zhai, R. Plebani, C. Y. Oh, M. Rodas, A. Patil, A. Nurani, S. E. Gilpin, R. K. Powers, G. Goyal, R. Prantil-Baun, D. E. Ingber, Mechanical control of innate immune responses against viral infection revealed in a human lung alveolus chip. *Nat. Commun.* **13**, 1928 (2022).
6. R. Pang, W. Sun, Y. Yang, D. Wen, F. Lin, D. Wang, K. Li, N. Zhang, J. Liang, C. Xiong, Y. Liu, PIEZO1 mechanically regulates the antitumour cytotoxicity of T lymphocytes. *Nat. Biomed. Eng.* **8**, 1162–1176 (2024).
7. M. Mukhopadhyay, Immunomechanics. *Nat. Methods* **20**, 35 (2023).
8. J. Rogers, A. T. Bajur, K. Salaita, K. M. Spillane, Mechanical control of antigen detection and discrimination by T and B cell receptors. *Biophys. J.* **123**, 2234–2255 (2024).
9. S. F. Mennens, K. van den Dries, A. Cambi, "Role for mechanotransduction in macrophage and dendritic cell immunobiology," in *Macrophages: Origin, Functions and Biointervention* (Springer International Publishing, 2017), pp. 209–242.
10. J. Li, X. Jiang, H. Li, M. Gelinsky, Z. Gu, Tailoring materials for modulation of macrophage fate. *Adv. Mater.* **33**, 2004172 (2021).
11. J. O. Abaricia, N. Farzad, T. J. Heath, J. Simmons, L. Morandini, R. Olivares-Navarrete, Control of innate immune response by biomaterial surface topography, energy, and stiffness. *Acta Biomater.* **133**, 58–73 (2021).
12. M. Chakraborty, K. Chu, A. Shrestha, X. S. Revelo, X. Zhang, M. J. Gold, S. Khan, M. Lee, C. Huang, M. Akbari, F. Barrow, Y. T. Chan, H. Lei, N. K. Kotoulas, J. Jovel, C. Pastrello, M. Kotlyar, C. Goh, E. Michelakis, X. Clemente-Casares, P. S. Ohashi, E. G. Engleman, S. Winer, I. Jurisica, S. Tsai, D. A. Winer, Mechanical stiffness controls dendritic cell metabolism and function. *Cell Rep.* **34**, 108609 (2021).
13. H. Rostam, S. Singh, N. Vrana, M. Alexander, A. Ghaemmaghami, Impact of surface chemistry and topography on the function of antigen presenting cells. *Biomater. Sci.* **3**, 424–441 (2015).
14. N. Jain, V. Vogel, Spatial confinement downsizes the inflammatory response of macrophages. *Nat. Mater.* **17**, 1134–1144 (2018).
15. K. M. Hotchkiss, G. B. Reddy, S. L. Hyzy, Z. Schwartz, B. D. Boyan, R. Olivares-Navarrete, Titanium surface characteristics, including topography and wettability, alter macrophage activation. *Acta Biomater.* **31**, 425–434 (2016).
16. X. Li, Q. Huang, T. A. Elkhooly, Y. Liu, H. Wu, Q. Feng, L. Liu, Y. Fang, W. Zhu, T. Hu, Effects of titanium surface roughness on the mediation of osteogenesis via modulating the immune response of macrophages. *Biomed. Mater.* **13**, 045013 (2018).
17. V. Bonito, B. J. de Kort, C. V. C. Bouten, A. I. P. M. Smits, Cyclic strain affects macrophage cytokine secretion and extracellular matrix turnover in electrospun scaffolds. *Tissue Eng. Part A* **25**, 1310–1325 (2019).
18. V. Ballotta, A. Driessen-Mol, C. V. C. Bouten, F. P. T. Baaijens, Strain-dependent modulation of macrophage polarization within scaffolds. *Biomaterials* **35**, 4919–4928 (2014).
19. E. Jui, G. Kingsley, H. K. T. Phan, K. L. Singampalli, R. K. Birla, J. P. Connell, S. G. Keswani, K. J. Grande-Allen, Shear stress induces a time-dependent inflammatory response in

Downloaded from https://www.science.org at EWHA Womans University on December 02, 2025

human monocyte-derived macrophages. bioRxiv 519590 [Preprint] (2022). https://doi.org/10.1101/2022.12.08.519590.
20. H. Lei, Y. Pan, R. Wu, Y. Lv, Innate immune regulation under magnetic fields with possible mechanisms and therapeutic applications. *Front. Immunol.* **11**, 582772 (2020).
21. K. Perica, A. Tu, A. Richter, J. G. Bieler, M. Edidin, J. P. Schneck, Magnetic field-induced T cell receptor clustering by nanoparticles enhances T cell activation and stimulates antitumor activity. *ACS Nano* **8**, 2252–2260 (2014).
22. M. Simkó, M. O. Mattsson, Extremely low frequency electromagnetic fields as effectors of cellular responses in vitro: Possible immune cell activation. *J. Cell. Biochem.* **93**, 83–92 (2004).
23. R. Li, J. C. Serrano, H. Xing, T. A. Lee, H. Azizgolshani, M. Zaman, R. D. Kamm, Interstitial flow promotes macrophage polarization toward an M2 phenotype. *Mol. Biol. Cell* **29**, 1927–1940 (2018).
24. Y. Kong, F. Liu, B. Ma, J. Duan, W. Yuan, Y. Sang, L. Han, S. Wang, H. Liu, Wireless localized electrical stimulation generated by an ultrasound-driven piezoelectric discharge regulates proinflammatory macrophage polarization. *Adv. Sci.* **8**, 2100962 (2021).
25. H. Shin, Fabrication methods of an engineered microenvironment for analysis of cell-biomaterial interactions. *Biomaterials* **28**, 126–133 (2007).
26. Y. Shao, J. Fu, Integrated micro/nanoengineered functional biomaterials for cell mechanics and mechanobiology: A materials perspective. *Adv. Mater.* **26**, 1494–1533 (2014).
27. M. Huse, Mechanical forces in the immune system. *Nat. Rev. Immunol.* **17**, 679–690 (2017).
28. Y. Shou, X. Y. Teo, K. Z. Wu, B. Bai, A. R. K. Kumar, J. Low, Z. Le, A. Tay, Dynamic stimulations with bioengineered extracellular matrix-mimicking hydrogels for mechano cell reprogramming and therapy. *Adv. Sci.* **10**, 2300670 (2023).
29. X. Wan, Z. Liu, L. Li, Manipulation of stem cells fates: The master and multifaceted roles of biophysical cues of biomaterials. *Adv. Funct. Mater.* **31**, 2010626 (2021).
30. T. Hodgkinson, P. M. Tsimbouri, V. Llopis-Hernandez, P. Campsie, D. Scurr, P. G. Childs, D. Phillips, S. Donnelly, J. A. Wells, F. J. O'Brien, M. Salmeron-Sanchez, K. Burgess, M. Alexander, M. Vassalli, R. O. C. Oreffo, S. Reid, D. J. France, M. J. Dalby, The use of nanovibration to discover specific and potent bioactive metabolites that stimulate osteogenic differentiation in mesenchymal stem cells. *Sci. Adv.* **7**, eabb7921 (2021).
31. P. M. Tsimbouri, P. G. Childs, G. D. Pemberton, J. Yang, V. Jayawarna, W. Orapiriyakul, K. Burgess, C. González-García, G. Blackburn, D. Thomas, C. Vallejo-Giraldo, M. J. P. Biggs, A. S. G. Curtis, M. Salmerón-Sánchez, S. Reid, M. J. Dalby, Stimulation of 3D osteogenesis by mesenchymal stem cells using a nanovibrational bioreactor. *Nat. Biomed. Eng.* **1**, 758–770 (2017).
32. H. Nikukar, S. Reid, P. M. Tsimbouri, M. O. Riehle, A. S. G. Curtis, M. J. Dalby, Osteogenesis of mesenchymal stem cells by nanoscale mechanotransduction. *ACS Nano* **7**, 2758–2767 (2013).
33. L. A. Ambattu, S. Ramesan, C. Dekiwadia, E. Hanssen, H. Li, L. Y. Yeo, High frequency acoustic cell stimulation promotes exosome generation regulated by a calcium-dependent mechanism. *Commun. Biol.* **3**, 553 (2020).
34. S. Yoo, D. R. Mittelstein, R. C. Hurt, J. Lacroix, M. G. Shapiro, Focused ultrasound excites cortical neurons via mechanosensitive calcium accumulation and ion channel amplification. *Nat. Commun.* **13**, 493 (2022).
35. C. Sun, Y. Dong, J. Wei, M. Cai, D. Liang, Y. Fu, Y. Zhou, Y. Sui, F. Wu, R. Mikhaylov, H. Wang, F. Fan, Z. Xie, M. Stringer, Z. Yang, Z. Wu, L. Tian, X. Yang, Acoustically accelerated neural differentiation of human embryonic stem cells. *Acta Biomater.* **151**, 333–345 (2022).
36. P. Xia, Y. Shi, X. Wang, X. Li, Advances in the application of low-intensity pulsed ultrasound to mesenchymal stem cells. *Stem Cell Res. Ther.* **13**, 214 (2022).
37. X. Li, Y. Zhong, W. Zhou, Y. Song, W. Li, Q. Jin, T. Gao, L. Zhang, M. Xie, Low-intensity pulsed ultrasound (LIPUS) enhances the anti-inflammatory effects of bone marrow mesenchymal stem cells (BMSCs)-derived extracellular vesicles. *Cell. Mol. Biol. Lett.* **28**, 9 (2023).
38. X. Jiang, O. Savchenko, Y. Li, S. Qi, T. Yang, W. Zhang, J. Chen, A review of low-intensity pulsed ultrasound for therapeutic applications. *IEEE Trans. Biomed. Eng.* **66**, 2704–2718 (2018).
39. G. Sitters, D. Kamsma, G. Thalhammer, M. Ritsch-Marte, E. J. G. Peterman, G. J. L. Wuite, Acoustic force spectroscopy. *Nat. Methods* **12**, 47–50 (2015).
40. S. Kwon, W. Yang, D. Moon, K. S. Kim, Comparison of cancer cell elasticity by cell type. *J. Cancer* **11**, 5403 (2020).
41. X. Zhang, T.-H. Kim, T. J. Thauland, H. Li, F. S. Majedi, C. Ly, Z. Gu, M. J. Butte, A. C. Rowat, S. Li, Unraveling the mechanobiology of immune cells. *Curr. Opin. Biotechnol.* **66**, 236–245 (2020).
42. J. Rufo, F. Cai, J. Friend, M. Wiklund, T. J. Huang, Acoustofluidics for biomedical applications. *Nat. Rev. Methods Primers* **2**, 30 (2022).
43. J. Rufo, P. Zhang, R. Zhong, L. P. Lee, T. J. Huang, A sound approach to advancing healthcare systems: The future of biomedical acoustics. *Nat. Commun.* **13**, 3459 (2022).
44. S. Yang, Z. Tian, Z. Wang, J. Rufo, P. Li, J. Mai, J. Xia, H. Bachman, P.-H. Huang, M. Wu, C. Chen, L. P. Lee, T. J. Huang, Harmonic acoustics for dynamic and selective particle manipulation. *Nat. Mater.* **21**, 540–546 (2022).
45. L.-X. Wang, S.-X. Zhang, H.-J. Wu, X.-L. Rong, J. Guo, M2b macrophage polarization and its roles in diseases. *J. Leukoc. Biol.* **106**, 345–358 (2019).
46. M. Wu, Z. Ma, Z. Tian, J. T. Rich, X. He, J. Xia, Y. He, K. Yang, S. Yang, K. W. Leong, L. P. Lee, T. J. Huang, Sound innovations for biofabrication and tissue engineering. *Microsyst. Nanoeng.* **10**, 170 (2024).
47. S. Zhao, Z. Tian, C. Shen, S. Yang, J. Xia, T. Li, Z. Xie, P. Zhang, L. P. Lee, S. A. Cummer, T. J. Huang, Topological acoustofluidics. *Nat. Mater.* **24**, 707–715 (2025).
48. Y. Gu, C. Chen, Z. Mao, H. Bachman, R. Becker, J. Rufo, Z. Wang, P. Zhang, J. Mai, S. Yang, J. Zhang, S. Zhao, Y. Ouyang, D. T. W. Wong, Y. Sadovsky, T. J. Huang, Acoustofluidic centrifuge for nanoparticle enrichment and separation. *Sci. Adv.* **7**, eabc0467 (2021).
49. A. Sica, M. Erreni, P. Allavena, C. Porta, Macrophage polarization in pathology. *Cell. Mol. Life Sci.* **72**, 4111–4126 (2015).
50. Y.-C. Liu, X.-B. Zou, Y.-F. Chai, Y.-M. Yao, Macrophage polarization in inflammatory diseases. *Int. J. Biol. Sci.* **10**, 520 (2014).
51. F. Y. McWhorter, T. Wang, P. Nguyen, T. Chung, W. F. Liu, Modulation of macrophage phenotype by cell shape. *Proc. Natl. Acad. Sci. U.S.A.* **110**, 17253–17258 (2013).
52. T. Topal, X. Hong, X. Xue, Z. Fan, N. Kanetkar, J. T. Nguyen, J. Fu, C. X. Deng, P. H. Krebsbach, Acoustic tweezing cytometry induces rapid initiation of human embryonic stem cell differentiation. *Sci. Rep.* **8**, 12977 (2018).
53. X. Xue, X. Hong, Z. Li, C. X. Deng, J. Fu, Acoustic tweezing cytometry enhances osteogenesis of human mesenchymal stem cells through cytoskeletal contractility and YAP activation. *Biomaterials* **134**, 22–30 (2017).
54. C. R. Below, J. Kelly, A. Brown, J. D. Humphries, C. Hutton, J. Xu, B. Y. Lee, C. Cintas, X. Zhang, V. Hernandez-Gordillo, L. Stockdale, M. A. Goldsworthy, J. Geraghty, L. Foster, D. A. O'Reilly, B. Schedding, J. Askari, J. Burns, N. Hodson, D. L. Smith, C. Lally, G. Ashton, D. Knight, A. Mironov, A. Banyard, J. A. Eble, J. P. Morton, M. J. Humphries, L. G. Griffith, C. Jørgensen, A microenvironment-inspired synthetic three-dimensional model for pancreatic ductal adenocarcinoma organoids. *Nat. Mater.* **21**, 110–119 (2022).
55. Z. Tong, R. L. Duncan, X. Jia, Modulating the behaviors of mesenchymal stem cells via the combination of high-frequency vibratory stimulations and fibrous scaffolds. *Tissue Eng. Part A* **19**, 1862–1878 (2013).
56. H. Kang, D. S. H. Wong, X. Yan, H. J. Jung, S. Kim, S. Lin, K. Wei, G. Li, V. P. Dravid, L. Bian, Remote control of multimodal nanoscale ligand oscillations regulates stem cell adhesion and differentiation. *ACS Nano* **11**, 9636–9649 (2017).
57. H. Deng, Z. Li, Y. Tan, Z. Guo, Y. Liu, Y. Wang, Y. Yuan, R. Yang, Y. Bi, Y. Bai, F. Zhi, A novel strain of *Bacteroides fragilis* enhances phagocytosis and polarises M1 macrophages. *Sci. Rep.* **6**, 29401 (2016).
58. C. Yunna, H. Mengru, W. Lei, C. Weidong, Macrophage M1/M2 polarization. *Eur. J. Pharmacol.* **877**, 173090 (2020).

Acknowledgments: We gratefully acknowledge the technical support provided by M. Pineda and D. Damiani of Polytec Inc. for guidance and contribution to the vibration measurements and analysis. We used ChatGPT (OpenAI) to help improve the clarity and readability of part of the manuscript after the initial draft was completed. **Funding:** We recognize the support from the National Institutes of Health (T.J.H: R01AG084098 and R01GM141055). **Author contributions:** Conceptualization: Y.H., K.J., J.X., Y.C., L.P.L., and T.J.H. Supervision: S.Y., Y.C., L.P.L., and T.J.H. Writing—original draft: Y.H., M.L., S.Y., Y.C., X.X., and L.P.L. Writing—review and editing: Y.H., K.J., B.P., J.D.H.M., X.X., Y.C., K.S., M.L., S.Y., J.X., L.P.L., and T.J.H. Investigation: Y.H., K.J., B.P., K.S., Y.C., and L.P.L. Validation: Y.H., B.P., Y.C., K.S., J.X., L.P.L., and T.J.H. Methodology: Y.H., K.J., X.X., Y.C., K.Y., J.X., Y.W., and L.P.L. Resources: B.P., Z.M., K.L., Y.C., Y.W., and T.J.H. Data curation: Y.H., B.P., Y.C., and L.P.L. Formal analysis: Y.H., B.P., K.L., X.X., Y.C., Z.M., and L.P.L. Software: B.P., J.X., X.X., and Y.C. Visualization: Y.H., B.P., K.L., Y.C., K.S., S.Y., M.L., J.X., and L.P.L. Funding acquisition: Y.C., L.P.L., and T.J.H. Project administration: Y.C., L.P.L., and T.J.H. **Competing interests:** T.J.H. has cofounded a start-up company, Ascent Bio-Nano Technologies Inc., to commercialize technologies involving acoustofluidics and acoustic tweezers. The authors declare that they have no other competing interests. **Data and materials availability:** All data needed to evaluate the conclusions in the paper are present in the paper and/or the Supplementary Materials. No special code was developed for this project.

Submitted 12 March 2025
Accepted 11 July 2025
Published 13 August 2025
10.1126/sciadv.adx3851

Downloaded from https://www.science.org at EWHA Womans University on December 02, 2025